

Focusing of atomic beams by near-field atom microlenses: The Bethe-type and the Fresnel-type microlenses

V. I. Balykin and V. G. Minogin*

Institute of Spectroscopy, Russian Academy of Sciences, 142190 Troitsk, Moscow Region, Russia

(Received 5 June 2007; published 2 January 2008)

We analyze focusing of atomic beams by the atom near-field microlenses produced by the laser fields diffracted on the apertures in the metallic screens. Analysis of the focusing properties of the atom microlenses is given in a model describing dipole interaction of atoms with a far-off-resonance laser light. Two types of the atom microlenses are considered: The Bethe-type microlens with aperture less than the light wavelength and the Fresnel-type microlens with aperture about the wavelength. It is shown that both types of the atom microlenses are able to produce strong dipole gradient forces which can focus the atomic beams. However, while the Bethe-atom microlens is able to produce sharp focusing of the beams the Fresnel-atom microlens possesses weak focusing property due to high anharmonicity of the gradient force. We conclude that the Bethe-atom microlens can be considered as a promising tool of the atom optics potentially able to focus atomic beams into spot sizes about nanometers.

DOI: [10.1103/PhysRevA.77.013601](https://doi.org/10.1103/PhysRevA.77.013601)

PACS number(s): 03.75.Be, 37.10.Vz, 37.10.De, 37.10.Gh

I. INTRODUCTION

In past years there is a growing number of experimental studies on focusing of atomic beams by laser light. Focused atomic beams are of interest for various applications including atom optics, microfabrication and nanofabrication, and atom lithography with nanometer resolution. Optical techniques have already been applied for focusing of atomic beams by Gaussian laser beams [1,2], hollow laser beams [3–8], and standing waves of the laser light [9–17]. A new and insufficiently studied approach to atomic beam focusing involves the atom near-field microlenses formed by the optical fields existing in the vicinity of small apertures in metallic screens [18,19]. This approach is interesting in view of the possibility of fabricating a large set of the atom microlenses and, accordingly, the possibility of producing a large set of the atom microbeams from a single initial atomic beam.

As in other approaches employing laser fields, the focusing properties of the atom near-field microlenses are based on the use of the dipole gradient force. However, in contrast to other approaches, in which the gradient force is due to the nonuniform field distribution over the laser beam cross section or over the wavelength of the laser light, the gradient force in the atom microlenses is associated with the optical field nonuniformity over the aperture diameter. Consequently, an atom microlens with a diameter smaller than or about the field wavelength may produce an atomic microbeam with a small diameter, while a set of near-field microlenses can produce a large number of microbeams. The latter can be used for preparing microstructures and nanostructures on substrates.

The scheme of a near-field atomic focusing was previously considered on the basis of a qualitative analysis of the effective atomic potential in a diffracted optical field [18,19]. The analysis revealed that effective focusing can be obtained

for relatively slow atomic beams. For a high velocity of atoms, short time of interaction of the atoms with the laser field limits the focusing ability of the near-field atom lenses.

This study aims at quantitative analysis of focusing properties of the atom near-field microlenses whose diameter is smaller than or about the wavelength of the optical field. For this purpose, we analyze the field distribution in the vicinity of a small aperture in a metallic screen and calculate the dipole gradient force on an atom in the diffracted field. The gradient force is used for numerical analysis of atomic trajectories in the near-field atom microlenses and for obtaining analytical estimates of the microlenses parameters.

We present an analysis of the two types of the atom microlenses: The Bethe-type microlens with aperture size less than the light wavelength and the Fresnel-type microlens with aperture size about the wavelength. Analysis of the Bethe-atom microlens is based on the known analytical solution of the problem of diffraction of a plane electromagnetic wave on a small-radius circular aperture in an infinitely large metallic screen [20–27]. Bethe [20] was the first who worked at this problem; the analytical solution to this problem was obtained in the final form by Bouwkamp [21,22]. Consideration of the Fresnel-atom microlens is based on numerical and analytical analysis of the Rayleigh-Sommerfeld diffraction formula.

II. BETHE-ATOM MICROLENS

Scheme of the Bethe-atom microlens is shown in Fig. 1(a). In this scheme, laser light is incident from the left on a conducting screen with a circular aperture with radius a considered to be smaller than the light wavelength λ . An atomic beam is also incident from the left on the screen with an aperture and is focused by the gradient force.

We assume that the electromagnetic field of the incident laser light is defined by the field vectors $\mathbf{E}'_0(\mathbf{r}, t)$ and $\mathbf{H}'_0(\mathbf{r}, t)$, while the electromagnetic field of the light reflected from the screen in the absence of the aperture is defined by field vectors $\mathbf{E}''_0(\mathbf{r}, t)$ and $\mathbf{H}''_0(\mathbf{r}, t)$. Accordingly, in the absence of the

*minogin@isan.troitsk.ru

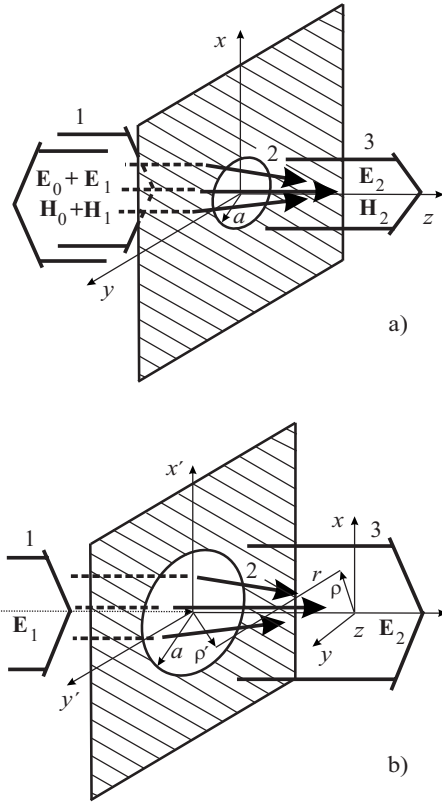


FIG. 1. (a) Bethe-type atom microlens. 1: the field produced by the incident laser light and the light reflected from the aperture, 2: focused atomic beam, 3: the field of the light transmitted through the aperture. (b) Fresnel-type atom microlens. 1: the incident laser light, 2: focused atomic beam, 3: the field of the light transmitted through the aperture.

aperture total electromagnetic field on the left of the screen is as

$$\mathbf{E}_0 = \mathbf{E}'_0 + \mathbf{E}''_0, \quad \mathbf{H}_0 = \mathbf{H}'_0 + \mathbf{H}''_0, \quad (1)$$

and on the right of the screen the field is equal to zero. In the presence of a small aperture in the screen, the electromagnetic field can be represented according to Bethe [20]. In the region on the left of the screen, i.e., at $z < 0$, the electromagnetic field can be represented as a sum of the unperturbed field and the field produced by the aperture

$$\mathbf{E}_l = \mathbf{E}_0 + \mathbf{E}_1, \quad \mathbf{H}_l = \mathbf{H}_0 + \mathbf{H}_1. \quad (2)$$

In the region on the right of the screen, i.e., at $z > 0$, the electromagnetic field can be represented as the field of the light transmitted through the aperture

$$\mathbf{E}_r = \mathbf{E}_2, \quad \mathbf{H}_r = \mathbf{H}_2. \quad (3)$$

In the case of linear polarization of incident light, analytical solutions are known for the above representation of the field, which are valid to the second order in small parameter ka , where $k = 2\pi/\lambda$ is the wave vector of the light [21,22]. These solutions can be written in a convenient form if one introduces coordinates u , v , and φ of an oblate ellipsoid of revolution

$$x = a(1 - u^2)^{1/2}(1 + v^2)^{1/2} \cos \varphi,$$

(4) $y = a(1 - u^2)^{1/2}(1 + v^2)^{1/2} \sin \varphi$, $z = auv$, where $0 \leq u \leq 1$, $-\infty \leq v \leq +\infty$, $0 \leq \varphi \leq 2\pi$. Coordinates u, v, φ being expressed in terms of the Cartesian coordinates are as

$$u = \frac{1}{\sqrt{2a}} \{a^2 - r^2 + [(a^2 - r^2)^2 + 4a^2 z^2]^{1/2}\}^{1/2},$$

$$v = \sqrt{2z} \{a^2 - r^2 + [(a^2 - r^2)^2 + 4a^2 z^2]^{1/2}\}^{-1/2}, \quad \varphi = \arctg(y/x), \quad (5)$$

where $r = (x^2 + y^2 + z^2)^{1/2}$.

Using introduced coordinates, we write out below the field vectors for linearly polarized incident light wave [21]. Then, we represent circularly polarized light wave as a sum of two linearly polarized waves and, applying the Bouwkamp formulas twice, write out the field vectors for circularly polarized incident wave. These results are used to find the energy density of the field and the dipole gradient force on the atom.

A. Electromagnetic field

1. Linear polarization

We choose first the incident laser light in the form of a plane traveling linearly polarized wave and write the electric vector of the wave in the form

$$\mathbf{E}'_0 = \mathbf{e}_x A \cos(kz - \omega t), \quad (6)$$

where \mathbf{e}_x is the unit vector along the Ox axis, A is the amplitude, and $k = \omega/c$ is the wave vector. The intensity of incident wave (6) is $I_0 = cA^2/8\pi$.

If there were no aperture in the metallic screen, incident wave (6) would produce a reflected wave with an electric vector

$$\mathbf{E}''_0 = -\mathbf{e}_x A \cos(kz + \omega t). \quad (7)$$

Thus, in the absence of an aperture, the electromagnetic field on the left of the screen is represented by a standing light wave

$$\mathbf{E}_0 = \mathbf{E}'_0 + \mathbf{E}''_0 = 2\mathbf{e}_x A \sin kz \sin \omega t, \quad (8)$$

$$\mathbf{H}_0 = \mathbf{H}'_0 + \mathbf{H}''_0 = 2\mathbf{e}_y A \cos kz \cos \omega t, \quad (9)$$

while the electromagnetic field on the right of the screen is equal to zero.

When a small aperture of radius a exists in the screen, the Cartesian components of the field vectors \mathbf{E}_r and \mathbf{H}_r on the right of the screen can be written as

$$E_{ri} = A \mathcal{E}_{ri} \sin \omega t, \quad (10)$$

$$H_{ri} = A \mathcal{H}_{ri} \cos \omega t, \quad (11)$$

where $i = x, y, z$. Dimensionless amplitudes of the electric field components entering Eq. (10) have the form [21]

$$\mathcal{E}_{rx} = kz - \frac{2}{\pi}kau \left[1 + v \operatorname{arctg} v + \frac{1}{3(u^2 + v^2)} + \frac{x^2 - y^2}{3a^2(u^2 + v^2)(1 + v^2)^2} \right],$$

$$\mathcal{E}_{ry} = -\frac{4}{3\pi a(u^2 + v^2)(1 + v^2)^2} kxyu, \quad \mathcal{E}_{rz} = \frac{4}{3\pi (u^2 + v^2)(1 + v^2)^2} kxv. \quad (12)$$

Dimensionless amplitudes of the magnetic field components entering Eq. (11) have the form

$$\mathcal{H}_{rx} = -\frac{4}{\pi a^2(u^2 + v^2)(1 + v^2)^2} xyv,$$

$$\mathcal{H}_{ry} = 1 - \frac{2}{\pi} \left[\operatorname{arctg} v + \frac{v}{u^2 + v^2} - \frac{(x^2 - y^2)v}{a^2(u^2 + v^2)(1 + v^2)^2} \right],$$

$$\mathcal{H}_{rz} = -\frac{4}{\pi a(u^2 + v^2)(1 + v^2)^2} yu. \quad (13)$$

The Cartesian components of the field vectors \mathbf{E}_l and \mathbf{H}_l on the left of the screen can be written in an analogous form

$$E_{li} = A\mathcal{E}_{li} \sin \omega t, \quad (14)$$

$$H_{li} = A\mathcal{H}_{li} \cos \omega t. \quad (15)$$

In Eq. (14) dimensionless electric field components have the form

$$\mathcal{E}_{lx} = 2 \sin kz - kz - \frac{2}{\pi}kau \left[1 + v \operatorname{arctg} v + \frac{1}{3(u^2 + v^2)} + \frac{x^2 - y^2}{3a^2(u^2 + v^2)(1 + v^2)^2} \right],$$

$$\mathcal{E}_{ly} = -\frac{4}{3\pi a(u^2 + v^2)(1 + v^2)^2} kxyu,$$

$$\mathcal{E}_{lz} = \frac{4}{3\pi (u^2 + v^2)(1 + v^2)^2} kxv. \quad (16)$$

Dimensionless magnetic field components entering Eq. (15) are given by

$$\mathcal{H}_{lx} = -\frac{4}{\pi a^2(u^2 + v^2)(1 + v^2)^2} xyv,$$

$$\mathcal{H}_{ly} = 2 \cos kz - 1 - \frac{2}{\pi} \left[\operatorname{arctg} v + \frac{v}{u^2 + v^2} - \frac{(x^2 - y^2)v}{a^2(u^2 + v^2)(1 + v^2)^2} \right],$$

$$\mathcal{H}_{lz} = -\frac{4}{\pi a(u^2 + v^2)(1 + v^2)^2} yu. \quad (17)$$

It should be emphasized that coordinates u and v in the above formulas can be expressed in terms of the Cartesian coordinates x and y according to Eq. (5).

2. Circular polarization

Consider now a case of a circular polarized incident light wave. The electric field of the incident wave assumed for definiteness to be left polarized wave can be chosen in the form

$$\mathbf{E}'_0 = \frac{1}{2}A[\mathbf{e}_+e^{i(kz-\omega t)} - \mathbf{e}_-e^{-i(kz-\omega t)}]$$

$$= -\frac{1}{\sqrt{2}}A[\mathbf{e}_x \cos(kz - \omega t) - \mathbf{e}_y \sin(kz - \omega t)], \quad (18)$$

where $\mathbf{e}_\pm = \mp \frac{1}{\sqrt{2}}(\mathbf{e}_x \pm i\mathbf{e}_y)$ are the spherical unit vectors. The intensity I_0 of the incident circularly polarized wave (18) is chosen to coincide with the intensity of a linearly polarized wave (6), $I_0 = cA^2/8\pi$.

In the absence of an aperture in the screen, incident wave (18) produces a reflected wave with the electric field

$$\mathbf{E}''_0 = -\frac{1}{2}A[\mathbf{e}_+e^{-i(kz+\omega t)} - \mathbf{e}_-e^{i(kz+\omega t)}]$$

$$= \frac{1}{\sqrt{2}}A[\mathbf{e}_x \cos(kz + \omega t) + \mathbf{e}_y \sin(kz + \omega t)]. \quad (19)$$

Accordingly, in the absence of the aperture in the screen the field on the left of the screen is described by a standing light wave

$$\mathbf{E}_0 = \mathbf{E}'_0 + \mathbf{E}''_0 = -\sqrt{2}A \sin kz(\mathbf{e}_x \sin \omega t - \mathbf{e}_y \cos \omega t), \quad (20)$$

$$\mathbf{H}_0 = \mathbf{H}'_0 + \mathbf{H}''_0 = \sqrt{2}A \cos kz(\mathbf{e}_x \sin \omega t - \mathbf{e}_y \cos \omega t), \quad (21)$$

while to the right of the screen the field is zero.

Note now that incident circular polarized wave (18) can be represented as a sum of two linearly polarized waves. One of them can be obtained from linearly polarized wave (6) by substitution

$$A \rightarrow -A/\sqrt{2}$$

and the other one by substitutions

$$A \rightarrow A/\sqrt{2}, \quad \omega t \rightarrow \omega t + \pi/2, \quad x \rightarrow y, \quad \mathbf{e}_x \rightarrow \mathbf{e}_y,$$

$$y \rightarrow -x, \quad \mathbf{e}_y \rightarrow -\mathbf{e}_x.$$

Accordingly, in the presence of the aperture in the screen, the diffracted electromagnetic field produced by the circular polarized incident wave can be found by applying the above substitutions to Eqs. (10)–(13) and Eqs. (14)–(17).

Taking into account the above substitutions one can represent the Cartesian components of electric field \mathbf{E}_r in the

region on the right of the screen in the convenient form

$$\begin{aligned} E_{rx} &= \frac{1}{\sqrt{2}}A(\mathcal{S}_{rx}^e \sin \omega t + \mathcal{C}_{rx}^e \cos \omega t), \\ E_{ry} &= \frac{1}{\sqrt{2}}A(\mathcal{S}_{ry}^e \sin \omega t + \mathcal{C}_{ry}^e \cos \omega t), \\ E_{rz} &= \frac{1}{\sqrt{2}}A(\mathcal{S}_{rz}^e \sin \omega t + \mathcal{C}_{rz}^e \cos \omega t), \end{aligned} \quad (22)$$

where dimensionless amplitudes of the electric field harmonics are as

$$\begin{aligned} \mathcal{S}_{rx}^e &= -kz + \frac{2}{\pi}kau \left[1 + v \operatorname{arctg} v + \frac{1}{3(u^2 + v^2)} \right. \\ &\quad \left. + \frac{x^2 - y^2}{3a^2(u^2 + v^2)(1 + v^2)^2} \right], \\ \mathcal{C}_{rx}^e &= -\mathcal{S}_{ry}^e = -\frac{4}{3\pi a(u^2 + v^2)(1 + v^2)^2} kxyu, \\ \mathcal{C}_{ry}^e &= kz - \frac{2}{\pi}kau \left[1 + v \operatorname{arctg} v + \frac{1}{3(u^2 + v^2)} \right. \\ &\quad \left. - \frac{x^2 - y^2}{3a^2(u^2 + v^2)(1 + v^2)^2} \right], \\ \mathcal{S}_{rz}^e &= -\frac{4}{3\pi(u^2 + v^2)(1 + v^2)} kxv, \\ \mathcal{C}_{rz}^e &= \frac{4}{3\pi(u^2 + v^2)(1 + v^2)} kyv. \end{aligned} \quad (23)$$

The Cartesian components of magnetic field \mathbf{H}_r in the region on the right of the screen can be written in analogous form

$$\begin{aligned} H_{rx} &= \frac{1}{\sqrt{2}}A(\mathcal{S}_{rx}^m \sin \omega t + \mathcal{C}_{rx}^m \cos \omega t), \\ H_{ry} &= \frac{1}{\sqrt{2}}A(\mathcal{S}_{ry}^m \sin \omega t + \mathcal{C}_{ry}^m \cos \omega t), \\ H_{rz} &= \frac{1}{\sqrt{2}}A(\mathcal{S}_{rz}^m \sin \omega t + \mathcal{C}_{rz}^m \cos \omega t), \end{aligned} \quad (24)$$

where dimensionless amplitudes of the magnetic field harmonics are as

$$\begin{aligned} \mathcal{S}_{rx}^m &= 1 - \frac{2}{\pi} \left[\operatorname{arctg} v + \frac{v}{u^2 + v^2} + \frac{(x^2 - y^2)v}{a^2(u^2 + v^2)(1 + v^2)^2} \right], \\ \mathcal{C}_{rx}^m &= -\mathcal{S}_{ry}^m = \frac{4}{\pi a^2(u^2 + v^2)(1 + v^2)^2} xyv, \\ \mathcal{C}_{ry}^m &= -1 + \frac{2}{\pi} \left[\operatorname{arctg} v + \frac{v}{u^2 + v^2} - \frac{(x^2 - y^2)v}{a^2(u^2 + v^2)(1 + v^2)^2} \right], \end{aligned}$$

$$\begin{aligned} \mathcal{S}_{rz}^m &= -\frac{4}{\pi a(u^2 + v^2)(1 + v^2)} xu, \\ \mathcal{C}_{rz}^m &= \frac{4}{\pi a(u^2 + v^2)(1 + v^2)} yu. \end{aligned} \quad (25)$$

The Cartesian components of electric field \mathbf{E}_l in the region on the left of the screen can be written in the form

$$\begin{aligned} E_{lx} &= \frac{1}{\sqrt{2}}A(\mathcal{S}_{lx}^e \sin \omega t + \mathcal{C}_{lx}^e \cos \omega t), \\ E_{ly} &= \frac{1}{\sqrt{2}}A(\mathcal{S}_{ly}^e \sin \omega t + \mathcal{C}_{ly}^e \cos \omega t), \\ E_{lz} &= \frac{1}{\sqrt{2}}A(\mathcal{S}_{lz}^e \sin \omega t + \mathcal{C}_{lz}^e \cos \omega t), \end{aligned} \quad (26)$$

where dimensionless amplitudes of the electric field harmonics have the form

$$\begin{aligned} \mathcal{S}_{lx}^e &= -2 \sin kz + kz + \frac{2}{\pi}kau \left[1 + v \operatorname{arctg} v + \frac{1}{3(u^2 + v^2)} \right. \\ &\quad \left. + \frac{x^2 - y^2}{3a^2(u^2 + v^2)(1 + v^2)^2} \right], \\ \mathcal{C}_{lx}^e &= -\mathcal{S}_{ly}^e = -\frac{4}{3\pi a(u^2 + v^2)(1 + v^2)^2} kxyu, \\ \mathcal{C}_{ly}^e &= 2 \sin kz - kz - \frac{2}{\pi}kau \left[1 + v \operatorname{arctg} v + \frac{1}{3(u^2 + v^2)} \right. \\ &\quad \left. - \frac{x^2 - y^2}{3a^2(u^2 + v^2)(1 + v^2)^2} \right], \\ \mathcal{S}_{lz}^e &= -\frac{4}{3\pi(u^2 + v^2)(1 + v^2)} kxv, \quad \mathcal{C}_{lz}^e = \frac{4}{3\pi(u^2 + v^2)(1 + v^2)} kyv. \end{aligned} \quad (27)$$

The Cartesian components of magnetic field \mathbf{H}_l in the region on the left of the screen can be written in analogous form

$$\begin{aligned} H_{lx} &= \frac{1}{\sqrt{2}}A(\mathcal{S}_{lx}^m \sin \omega t + \mathcal{C}_{lx}^m \cos \omega t), \\ H_{ly} &= \frac{1}{\sqrt{2}}A(\mathcal{S}_{ly}^m \sin \omega t + \mathcal{C}_{ly}^m \cos \omega t), \\ H_{lz} &= \frac{1}{\sqrt{2}}A(\mathcal{S}_{lz}^m \sin \omega t + \mathcal{C}_{lz}^m \cos \omega t), \end{aligned} \quad (28)$$

where dimensionless amplitudes of the magnetic field harmonics have the form

$$S_{lx}^m = 2 \cos kz - 1 - \frac{2}{\pi} \left[\arctg v + \frac{v}{u^2 + v^2} + \frac{(x^2 - y^2)v}{a^2(u^2 + v^2)(1 + v^2)^2} \right],$$

$$C_{lx}^m = -S_{ly}^m = \frac{4}{\pi} \frac{xyv}{a^2(u^2 + v^2)(1 + v^2)},$$

$$C_{ly}^m = -2 \cos kz + 1 + \frac{2}{\pi} \left[\arctg v + \frac{v}{u^2 + v^2} - \frac{(x^2 - y^2)v}{a^2(u^2 + v^2)(1 + v^2)^2} \right],$$

$$S_{lz}^m = -\frac{4}{\pi} \frac{xu}{a(u^2 + v^2)(1 + v^2)}, \quad C_{lz}^m = \frac{4}{\pi} \frac{yu}{a(u^2 + v^2)(1 + v^2)}. \quad (29)$$

Equations (22)–(25) completely define the electric and magnetic vectors of the diffracted light field in the region on the right of the screen. Equations (26)–(29) completely define the electric and magnetic vectors of the total light field in the region on the left of the screen.

B. Electric energy density

1. Linear polarization

For linearly polarized incident light wave when the Cartesian components of the diffracted light field are defined by Eqs. (10)–(17) the time average density of the electric field energy is as

$$w_\alpha = \frac{1}{8\pi} \langle \mathbf{E}_\alpha^2 \rangle_t = w_0 \sum_{i=x,y,z} \mathcal{E}_{\alpha i}^2, \quad (30)$$

where $\alpha=r$ stands for the region on the right of the screen, $\alpha=l$ stands for the region on the left of the screen, and $w_0 = A^2/16\pi = I_0/2c$ is the electric energy density in the incident light wave.

Making use of Eqs. (12) one can find the electric energy density on the right of the screen as

$$w_r = w_0 \left\{ \left[kz - \frac{2}{\pi} kau \left(1 + v \arctg v + \frac{1}{3(u^2 + v^2)} + \frac{x^2 - y^2}{3a^2(u^2 + v^2)(1 + v^2)^2} \right) \right]^2 + \left(\frac{4ka}{3\pi} \right)^2 \frac{x^2[y^2u^2 + a^2v^2(1 + v^2)^2]}{a^4(u^2 + v^2)^2(1 + v^2)^4} \right\}. \quad (31)$$

The electric energy density on the left of the screen can be found with the use of Eqs. (16) as

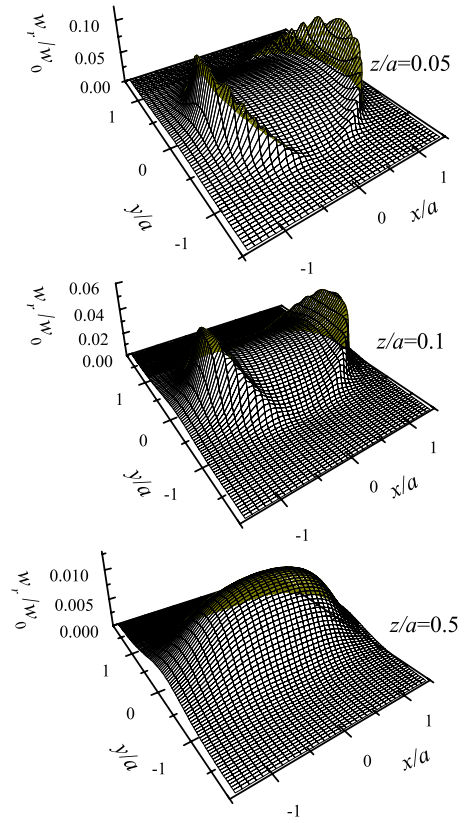


FIG. 2. (Color online) Electric energy density as a function of transverse coordinates in the case of incidence of a linearly polarized light wave on a screen with a circular aperture at $ka=0.25$ and at distances from the aperture $z=0.05a$, $0.1a$, and $0.5a$.

$$w_l = w_0 \left\{ \left[2 \sin kz - kz - \frac{2}{\pi} kau \left(1 + v \arctg v + \frac{1}{3(u^2 + v^2)} + \frac{x^2 - y^2}{3a^2(u^2 + v^2)(1 + v^2)^2} \right) \right]^2 + \left(\frac{4ka}{3\pi} \right)^2 \frac{x^2[y^2u^2 + a^2v^2(1 + v^2)^2]}{a^4(u^2 + v^2)^2(1 + v^2)^4} \right\}. \quad (32)$$

Figure 2 shows the electric energy density (31) referred to the region on the right of the screen as a function of transverse coordinates. It is worth noting that the density of the electric energy both transmitted through and reflected from the aperture includes two different parts. One of them comes from the internal region of the diffracted field which propagates inside the aperture but not to close to the edge of the aperture. This part is accordingly weakly perturbed by the edge diffraction. The other part comes from the outer region of the field strongly perturbed by diffraction on the edges of the aperture.

The presence of the above two parts in the diffracted field can be seen from equations for the field components if one takes into account that at the aperture edges the coordinates of the oblate ellipsoid of rotation are close to values $u=0$ and $v=0$. In accordance with this observation one can also rearrange the terms in Eqs. (31) and (32) and rewrite the electric energy density as

$$w_{r,l} = w_0 \left(\frac{2ka}{\pi} \right)^2 \left[u^2 \left(\Phi_{r,l}^2 + \frac{1}{9(1+v^2)^2} \right) + \frac{2u^2}{3} \left(\frac{2 \cos^2 \varphi}{u^2 + v^2} - \frac{\cos 2\varphi}{1+v^2} \right) \Phi_{r,l} + \frac{4(1-u^2)\cos^2 \varphi}{9(u^2+v^2)(1+v^2)} \right], \quad (33)$$

where

$$\Phi_r = 1 + v \left(\arctg v - \frac{\pi}{2} \right), \quad (34)$$

$$\Phi_l = 1 + v \left(\arctg v + \frac{\pi}{2} - \pi \frac{\sin kz}{kz} \right). \quad (35)$$

As one may now see, the first two terms in Eq. (33) define smooth variation of the energy density while the third term describes sharp variation near values of coordinates $u=0$, $v=0$, i.e., near the aperture edges. Note also that in the region far to the left of the screen the contribution of the small aperture is small and the electromagnetic field has a form of the standing wave described by Eqs. (8) and (9) with the electric energy density

$$w_l = 4w_0 \sin^2 kz.$$

2. Circular polarization

For circular polarized incident light wave the electric energy density averaged over time is as

$$w_\alpha = \frac{1}{8\pi} \langle \mathbf{E}_\alpha^2 \rangle_t = \frac{1}{2} w_0 \sum_{i=x,y,z} (S_{\alpha i}^2 + C_{\alpha i}^2), \quad (36)$$

where $\alpha=r$ refers for the region to the right of the screen, $\alpha=l$ for the region to the left of the screen, and $w_0 = A^2/16\pi = I_0/2c$ is the electric energy density in the incident light wave. Substituting amplitudes of the field harmonics (23) and (27) into the above equation one can see that the electric energy density is given by

$$w_r = w_0 \left\{ \left[kz - \frac{2}{\pi} kau \left(1 + v \arctg v + \frac{1}{3(u^2+v^2)} \right) \right]^2 + \left(\frac{2ka}{3\pi} \right)^2 \frac{(1-u^2)[u^2(1-u^2) + 2v^2(1+v^2)]}{(u^2+v^2)^2(1+v^2)^2} \right\} \quad (37)$$

for the region on the right of the screen and

$$w_l = w_0 \left\{ \left[2 \sin kz - kz - \frac{2}{\pi} kau \left(1 + v \arctg v + \frac{1}{3(u^2+v^2)} \right) \right]^2 + \left(\frac{2ka}{3\pi} \right)^2 \frac{(1-u^2)[u^2(1-u^2) + 2v^2(1+v^2)]}{(u^2+v^2)^2(1+v^2)^2} \right\} \quad (38)$$

for the region on the left of the screen.

Figure 3 shows dependence of the electric energy density w_r on transverse coordinates in the region on the right of the screen. Similar to electric energy density shown in Fig. 2 the electric energy density shown in Fig. 3 consists of two dif-

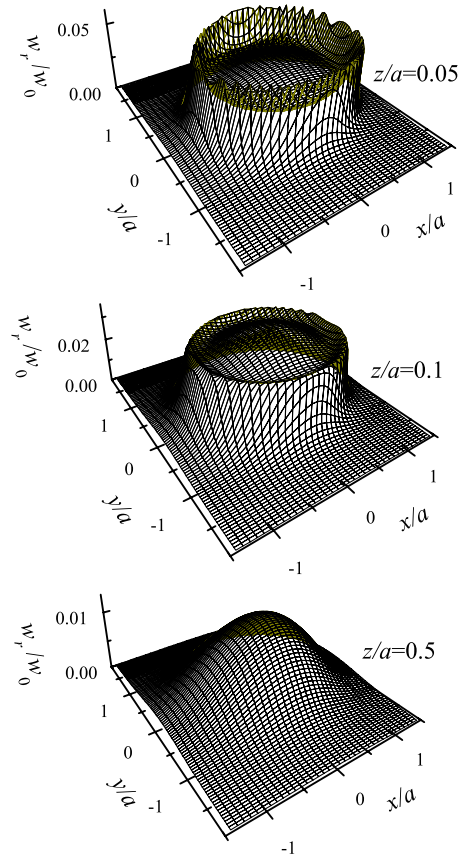


FIG. 3. (Color online) Electric energy density as a function of transverse coordinates in the case of incidence of a circularly polarized light wave on a screen with a circular aperture at $ka=0.25$ and at distances from the aperture $z=0.05a$, $0.1a$, and $0.5a$.

ferent parts. One part describes a smooth variation of the energy density within the aperture. This part is determined by the field propagating not too close to the edges of the aperture and, hence, slightly perturbed by the edge diffraction effect. The other part describes the sharp variation of the energy density due to the edge diffraction.

The presence of these two parts can be clearly seen if one rewrites the electric energy density in the form which takes into account the fact that the coordinates of the oblate ellipsoid of revolution at the aperture edges assume the values $u=0$, $v=0$. After that the electric energy density can be represented as

$$w_{r,l} = w_0 \left(\frac{2ka}{\pi} \right)^2 \left[u^2 \left(\Phi_{r,l}^2 + \frac{1}{9(1+v^2)^2} \right) + \frac{2u^2}{3(u^2+v^2)} \Phi_{r,l} + \frac{2(1-u^2)}{9(u^2+v^2)(1+v^2)} \right], \quad (39)$$

where functions $\Phi_{r,l}$ are defined by Eqs. (34) and (35). The first two terms in Eqs. (39) define the smooth variation of the electric energy density, while the last term is responsible for the sharp variation of energy density near coordinate values $u=0$ and $v=0$, i.e., at the aperture edges. Contributions of the different terms of Eqs. (39) are illustrated in Fig. 4 on the example of the electric energy density w_r .

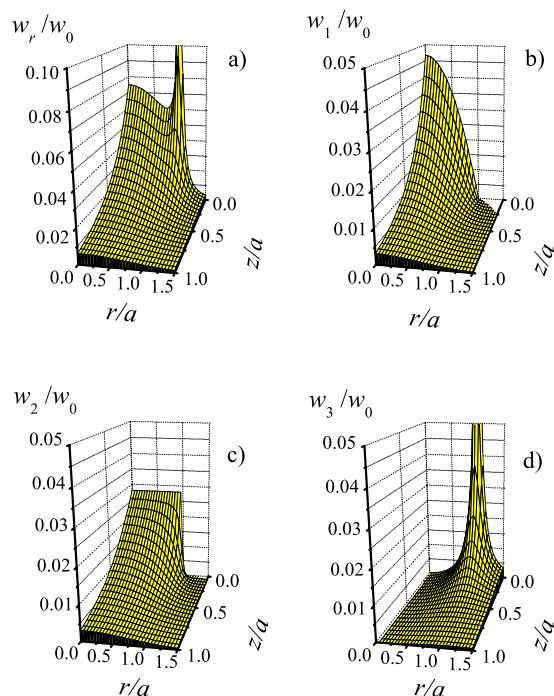


FIG. 4. (Color online) Electric energy density on the right of the screen in case of a circular polarized incident light wave at $ka = 0.25$ (a) and contributions to the electric energy density of the first (b), second (c), and third (d) term of Eq. (39).

It is worth noting that in full accordance with intuitive expectations energy density for circular polarized light can be obtained by averaging energy density for linear polarized light over the angle φ . Putting $\cos^2 \varphi = 1/2$ and $\sin^2 \varphi = 1/2$ one can see that Eq. (33) transforms into Eq. (39). Note finally that in the region on the left of the screen and at a large distance from the screen, i.e., in the region where the effect of the small aperture can be ignored, the electromagnetic field is reduced to a standing wave with the field vectors (20) and (21) and electric energy density

$$w_l = 4w_0 \sin^2 kz.$$

III. FRESNEL-ATOM MICROLENS

In the case of the Fresnel-atom microlens shown in Fig. 1(b) the radius a of the aperture in the metallic screen is assumed to be about or exceed the light wavelength $a \geq \lambda$. We consider the case of the Fresnel-atom microlens in sufficient for our purposes scalar approximation. Since in this approximation the electric and magnetic field are assumed to propagate in the same manner, in what follows we consider propagation of the electric field only.

Taking next into account that in the scalar approximation the diffraction process is insensitive to polarization we assume that the aperture in the screen is illuminated by a traveling laser wave of arbitrary polarization

$$\mathbf{E}_1 = \mathbf{e}E_0 \cos(kz - \omega t), \quad (40)$$

where \mathbf{e} is a unit polarization vector, E_0 is the amplitude, and $k = \omega/c$ the wave vector. Intensity of the incident wave (40) is $I_0 = cE_0^2/8\pi$.

A. Electromagnetic field

For the case of the Fresnel-atom microlens the electric field of the diffracted light can be represented in the scalar approximation as

$$\mathbf{E}_2 = \mathbf{e}E = \mathbf{e} \operatorname{Re}(\mathcal{E}e^{-i\omega t}), \quad (41)$$

where $\mathcal{E} = \mathcal{E}(\mathbf{r})$ is the complex field amplitude. The diffracted field can be calculated by applying the Rayleigh-Sommerfeld diffraction formula

$$\mathcal{E}(x, y, z) = \frac{1}{2\pi} \iint \mathcal{E}(x', y', 0) \frac{\exp(ikr)}{r} \left(\frac{z}{r}\right) \left(\frac{1}{r} - ik\right) dx' dy', \quad (42)$$

where the distance between the point x, y, z in the observation plane and the point $x', y', 0$ in the aperture plane shown in Fig. 1(b) is

$$r = [z^2 + (x - x')^2 + (y - y')^2]^{1/2}. \quad (43)$$

Amplitude of the field in the aperture plane according to a standard Kirchoff approximation is considered as $\mathcal{E}(x', y', 0) = E_0$ inside the aperture and $\mathcal{E}(x', y', 0) = 0$ outside the aperture.

To account for the axial symmetry of the scattered field we introduce cylindrical coordinates ρ', ϕ' in the aperture plane and ρ, ϕ in the observation plane and rewrite the electric field as

$$\mathcal{E}(\rho, z) = \frac{E_0}{2\pi} \int_0^a \int_0^{2\pi} \frac{\exp(ikr)}{r} \frac{z}{r} \left(\frac{1}{r} - ik\right) d\varphi \rho' d\rho', \quad (44)$$

where now

$$r = [z^2 + \rho^2 + \rho'^2 - 2\rho\rho' \cos \varphi]^{1/2}, \quad (45)$$

and $\varphi = \phi' - \phi$ is the relative angular coordinate. Alongside with above integral representation we derive additionally analytical representation of the electric field valid near the optical axis of symmetry. To do that we decompose the integrand in Eq. (44) into the series in small displacement $\rho \ll a$. Taking such a decomposition up to the fourth order in ρ we represent the distance between the point in the observation plane and the plane of the aperture as

$$\begin{aligned} r = & R - \frac{\rho' \cos \varphi}{R} \rho + \frac{1}{2R} \left(1 - \frac{\rho'^2 \cos^2 \varphi}{R^2}\right) \rho^2 \\ & + \frac{\rho' \cos \varphi}{2R^3} \left(1 - \frac{\rho'^2 \cos^2 \varphi}{R^2}\right) \rho^3 \\ & - \frac{1}{8R^3} \left(1 - \frac{6\rho'^2 \cos^2 \varphi}{R^2} + \frac{5\rho'^4 \cos^4 \varphi}{R^4}\right) \rho^4, \end{aligned} \quad (46)$$

where $R = (z^2 + \rho'^2)^{1/2}$.

After decomposition of the integrand in Eq. (44) the double integral is reduced to more simple ordinary integral

$$\begin{aligned} \mathcal{E}(\rho, z) = & -E_0 \int_z^{R_a} d \operatorname{Re} e^{ikR} \left(\frac{ikz}{R} A - \frac{z}{R^2} B + \frac{9ikz\rho^2}{4R^3} C - \frac{9z\rho^2}{4R^4} D \right. \\ & - \frac{15ikz^3\rho^2}{4R^5} E + \frac{15z^3\rho^2}{4R^6} F - \frac{525ikz^3\rho^4}{32R^7} G \\ & \left. + \frac{525z^3\rho^4}{32R^8} H + \frac{945ikz^5\rho^4}{64R^9} - \frac{945z^5\rho^4}{64R^{10}} \right), \end{aligned} \quad (47)$$

where $R_a = (z^2 + a^2)^{1/2}$ and A, B, C, \dots, H are the functions of the observation point,

$$\begin{aligned} A &= 1 - \frac{1}{4}k^2\rho^2 + \frac{1}{64}k^4\rho^4, & B &= 1 - k^2\rho^2 + \frac{7}{64}k^4\rho^4, \\ C &= 1 + \frac{1}{9}k^2z^2 - \frac{11}{48}k^2\rho^2 - \frac{1}{72}k^4z^2\rho^2, \\ D &= 1 + \frac{2}{3}k^2z^2 - \frac{3}{4}k^2\rho^2 - \frac{11}{72}k^4z^2\rho^2, \\ E &= 1 - \frac{15\rho^2}{16z^2} - \frac{13}{24}k^2\rho^2 - \frac{1}{240}k^4z^2\rho^2, \\ F &= 1 - \frac{15\rho^2}{16z^2} - 2k^2\rho^2 - \frac{1}{16}k^4z^2\rho^2, \\ G &= 1 + \frac{1}{10}k^2z^2, & H &= 1 + \frac{2}{5}k^2z^2. \end{aligned}$$

The last integral can be calculated by parts to give analytical expression for the diffracted electric field near the optical axis of the system as

$$\mathcal{E}(\rho, z) = E_0 \mathcal{I}, \quad (48)$$

where dimensionless function \mathcal{I} connects the diffracted and incident field as

$$\begin{aligned} \mathcal{I} = & e^{ikz} \left(1 - \frac{z}{R_a} e^{ik(R_a - z)} \right) + \frac{k^2 a^2 z \rho^2}{4R_a^3} \left(1 + \frac{3i}{kR_a} - \frac{3}{k^2 R_a^2} \right) e^{ikR_a} \\ & - \frac{k^4 a^4 z \rho^4}{64R_a^5} \left[1 + \frac{2i(3 - 2z^2/a^2)}{kR_a} - \frac{3(7 - 8z^2/a^2)}{k^2 R_a^2} \right. \\ & \left. - \frac{15i(3 - 4z^2/a^2)}{k^3 R_a^3} + \frac{15(3 - 4z^2/a^2)}{k^4 R_a^4} \right] e^{ikR_a}. \end{aligned} \quad (49)$$

Note that in the plane of the aperture, i.e., at $z=0$, the dimensionless function has a value of $\mathcal{I}=1$ and accordingly the diffracted field is equal to the incident field in accordance with the Kirhoff approximation. Note also that at $\rho=0$ Eq. (49) reduces to the equation found in Refs. [28,29], which treated the diffracted field on the optical axis, i.e., in zero order in small displacement ρ .

B. Electric energy density

For the diffracted field of the Fresnel-atom lens the electric energy density averaged over time is

$$w = \frac{1}{8\pi} \langle E^2 \rangle_t = \frac{1}{16\pi} |\mathcal{E}|^2. \quad (50)$$

Note that electric energy density for the incident laser wave is $w_0 = E_0^2 / 16\pi$.

At small displacement from the optical axis the electric energy density can be calculated with the use of Eqs. (48) and (49) as

$$w = w_0 \mathcal{J}, \quad (51)$$

where dimensionless function \mathcal{J} is defined up to the fourth order in small displacement ρ :

$$\begin{aligned} \mathcal{J} = & 1 + \frac{z^2}{R_a^2} - \frac{2z}{R_a} \cos k(R_a - z) - \frac{k^2 a^2 z \rho^2}{2R_a^3} \left[\left(1 - \frac{3}{k^2 R_a^2} \right) \left(\frac{z}{R_a} \right. \right. \\ & \left. \left. - \cos k(R_a - z) \right) + \frac{3}{kR_a} \sin k(R_a - z) \right] + \frac{k^4 a^4 z \rho^4}{32R_a^5} \left[\left(1 \right. \right. \\ & \left. \left. - \frac{3(7 - 8z^2/a^2)}{k^2 R_a^2} + \frac{15(3 - 4z^2/a^2)}{k^4 R_a^4} \right) \left(\frac{z}{R_a} - \cos k(R_a - z) \right) \right. \\ & \left. \left. + \frac{1}{kR_a} \left(2 \left(3 - 2 \frac{z^2}{a^2} \right) - \frac{15(3 - 4z^2/a^2)}{k^2 R_a^2} \right) \sin k(R_a - z) \right]. \end{aligned} \quad (52)$$

It is worth noting that in the plane of the aperture, i.e., at $z=0$ and $R_a=a$, the dimensionless function has a value of $\mathcal{J}=1$ and accordingly the electric energy density is equal to that of the incident light wave.

Typical distribution of the electric energy density over transverse coordinates for the Fresnel-atom lens is shown in Fig. 5. Distribution of the electric energy density over longitudinal and transverse coordinates is shown in Fig. 6. Figure 7 shows transverse profiles of the electric energy density at different values of the longitudinal coordinate z .

IV. GRADIENT FORCE

In the general case, the atoms moving through the aperture in the screen experience the action of the dipole force, which includes the gradient force of the potential type and the dissipative radiation pressure force [17,30]. At large negative detunings the gradient force produces nearly potential focusing of the atomic beam while radiation pressure force reduces to a small value. Accordingly, only the potential gradient force at large negative detuning is of interest for atomic focusing. Moreover, since the longitudinal velocities of atoms in the atomic beam considerably exceed the transverse velocities and accordingly longitudinal kinetic energies of the atoms exceed the transverse kinetic energies, the contribution of the longitudinal component of the gradient force to atomic trajectories is always smaller than that of the radial component of the gradient force. For these reasons, analysis of atomic beam focusing by near-field atom microlenses can be done by taking into account only the radial component of the gradient force.

The gradient force on an atom in a quasi-resonance laser field at large detunings exceeding both the homogeneous

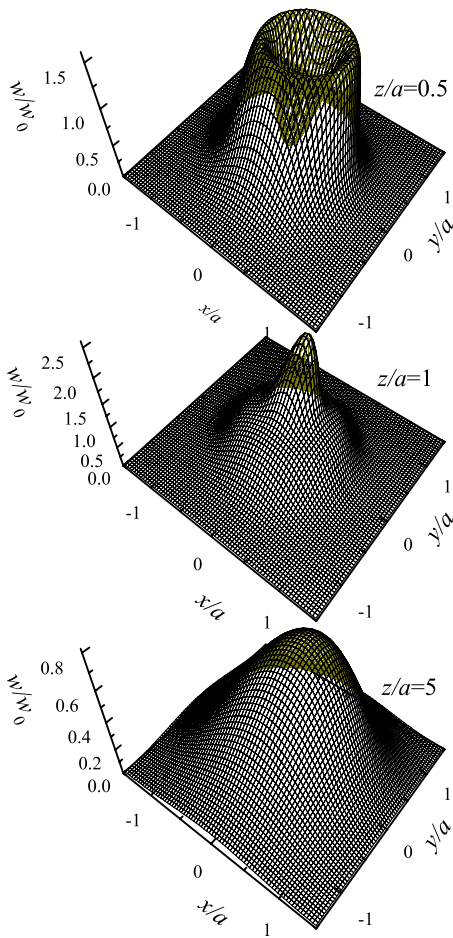


FIG. 5. (Color online) Electric energy density for the Fresnel-atom microlens at $ka=10$ and at distances from the screen $z=0.5a$, $z=1a$, and $z=5a$.

linewidth and the Doppler shift in a model of a two-level atom can be represented as [17,30]

$$\mathbf{F} = -\frac{\hbar\gamma^2}{2\delta} \nabla G, \quad (53)$$

where $\delta = \omega - \omega_0$ is the detuning of the light frequency with respect to the atomic transition frequency,

$$2\gamma = \frac{4d^2\omega_0^3}{3\hbar c^3} \quad (54)$$

is the spontaneous decay rate, and

$$G = \frac{1}{2} \left(\frac{dE}{\hbar\gamma} \right)^2$$

is the dimensionless saturation parameter. In the above equations d is the matrix element of the atomic dipole moment and E is the electric field amplitude at the location of the atom.

For large negative detunings the radial component of the gradient force has the form

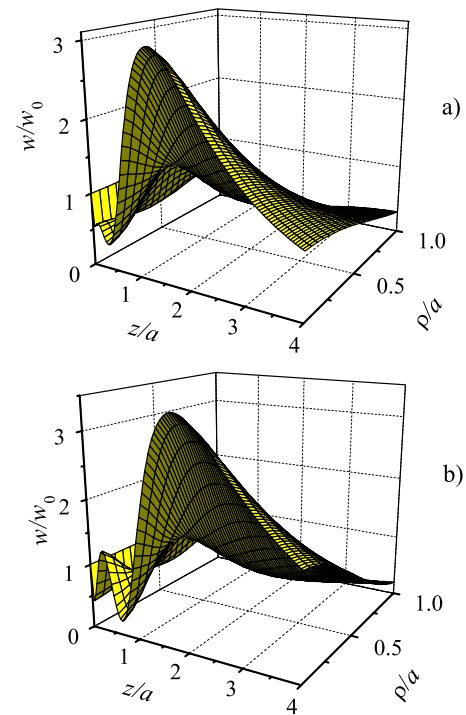


FIG. 6. (Color online) Electric energy density for the Fresnel-atom lens at $ka=8$ (a) and $ka=11$ (b).

$$F_\rho = \frac{\hbar\gamma^2}{2|\delta|} \frac{\partial G}{\partial \rho}, \quad (55)$$

where $\rho = (x^2 + y^2)^{1/2}$ is the radial coordinate. This force is directed toward the axis of the nonuniform optical field and is accordingly responsible for focusing of the atomic beam.

For subsequent analysis, it is convenient to express the saturation parameter in terms of the electric energy density

$$G = \frac{8\pi d^2 w}{\hbar^2 \gamma^2}$$

and take into account Eq. (54) for the spontaneous decay rate. After this, the radial component of the gradient force, which will be referred for brevity as the gradient force, assumes the convenient form

$$F_\rho = 6\pi \frac{\gamma}{|\delta|} \frac{1}{k^3} \frac{\partial w}{\partial \rho}, \quad (56)$$

where the electric energy density to the left of the screen is $w = w_l$ and to the right of the screen is $w = w_r$.

A. Bethe-atom microlens

In case of the Bethe-atom microlens and for a circular polarized incident laser wave the gradient force (56) can be represented in an explicit radial-symmetric form as

$$F_\rho = -F_0 \frac{\rho}{a} \eta(\rho, z), \quad (57)$$

where F_0 is a constant quantity having the dimension of force

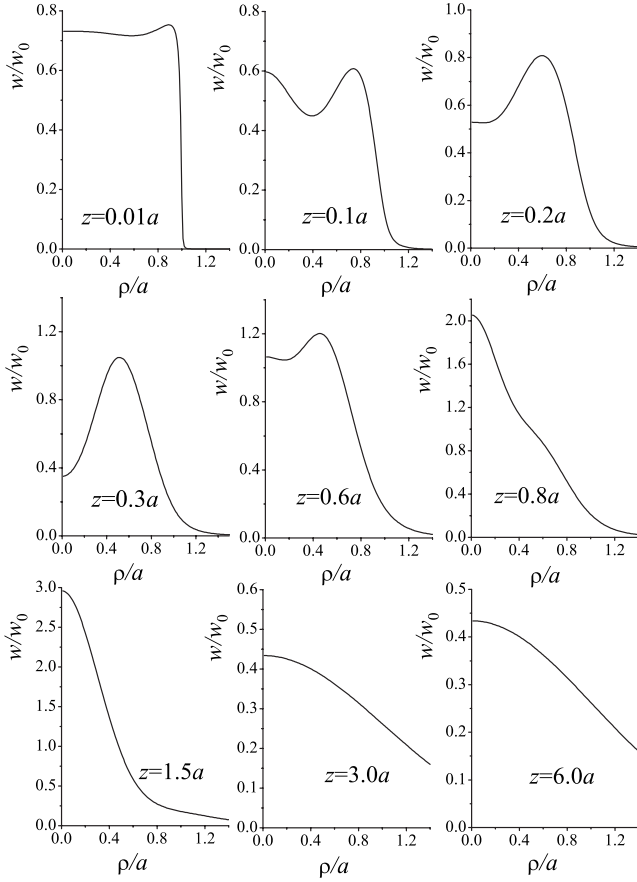


FIG. 7. Transverse profiles of the electric energy density for the Fresnel-atom microlens at $ka=8$ and different values of longitudinal coordinate z .

$$F_0 = \frac{24 I_0 a}{\pi \omega_0 |\delta|} \gamma, \quad (58)$$

$I_0 = cA^2/8\pi$ is the intensity of laser light incident on the screen, and $\eta(\rho, z)$ is the dimensionless function of coordinates, which is determined by the radial gradient of electric energy density. In the regions to the right and to the left of the screen, the dimensionless function $\eta = \eta_{r,l}(\rho, z)$ has a unified form

$$\begin{aligned} \eta_{r,l}(\rho, z) = & \frac{1}{(u^2 + v^2)} \left[\frac{u^2}{1 + v^2} \left(\Phi_{r,l} + \frac{1 + 3v^2}{9(1 + v^2)^2} \right) \right. \\ & + \frac{u^2}{3(u^2 + v^2)} \left(\frac{3v^2 - u^2}{u^2 + v^2} \Phi_{r,l} + \frac{1}{1 + v^2} \right) \\ & \left. + \frac{2}{9} \left(\frac{v^2 - u^2}{(u^2 + v^2)^2} - \frac{v^2}{(1 + v^2)^2} \right) \right]. \quad (59) \end{aligned}$$

We recall that the phase function $\Phi_{r,l}$ in the regions to the right and left of the screen is defined by Eq. (39). Dependence of the gradient force F_ρ on atomic coordinates is shown in Fig. 8.

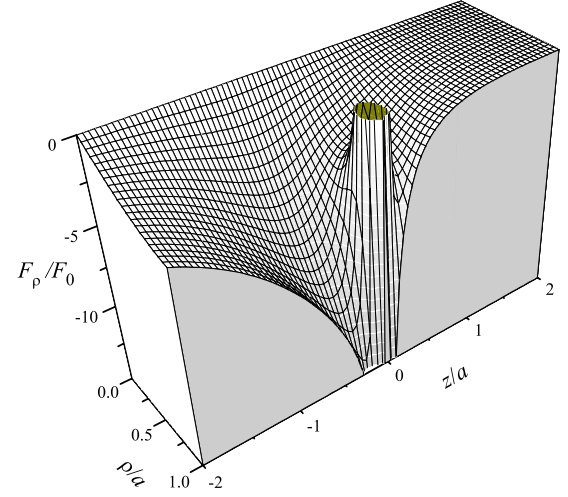


FIG. 8. (Color online) Radial component of the gradient force in case of the Bethe-atom microlens as a function of coordinates at $ka=0.25$ and for circular polarized incident laser wave.

B. Fresnel-atom microlens

In case of the Fresnel-atom microlens the gradient force is defined by Eq. (56) where electric energy density (50) can be evaluated with the use of Eq. (44). At small displacement from the symmetry axis the gradient force (56) is evaluated with the use of Eqs. (50)–(52) as

$$F_\rho = -\kappa(z)\rho + \mu(z)\rho^3, \quad (60)$$

where the “spring” constant and “anharmonicity” constant are

$$\begin{aligned} \kappa(z) = F_1 \frac{k^2 a^3 z}{R_a^3} \left[\left(1 - \frac{3}{k^2 R_a^2} \right) \left(\frac{z}{R_a} - \cos k(R_a - z) \right) \right. \\ \left. + \frac{3}{k R_a} \sin k(R_a - z) \right], \quad (61) \end{aligned}$$

$$\begin{aligned} \mu(z) = F_1 \frac{k^4 a^5 z}{8 R_a^5} \left\{ \left(1 - \frac{3(7 - 8z^2/a^2)}{k^2 R_a^2} + \frac{15(3 - 4z^2/a^2)}{k^2 R_a^2} \right) \right. \\ \times \left(\frac{z}{R_a} - \cos k(R_a - z) \right) + \frac{1}{k R_a} \left[2 \left(3 - 2 \frac{z^2}{a^2} \right) \right. \\ \left. \left. - \frac{15(3 - 4z^2/a^2)}{k^2 R_a^2} \right] \sin k(R_a - z) \right\}. \quad (62) \end{aligned}$$

In the above equations

$$F_1 = \frac{3\pi c^2 I_0}{a \omega_0^3 |\delta|} \gamma \quad (63)$$

is a typical value of the force and $I_0 = 2cw_0$ is the intensity of the incident light wave. Gradient force for the Fresnel-atom microlens is shown in Fig. 9 as a function of longitudinal and transverse coordinates.

V. ATOMIC BEAM FOCUSING

We compare properties of the Bethe- and Fresnel-atom microlenses by considering focusing of a beam of ^{85}Rb at

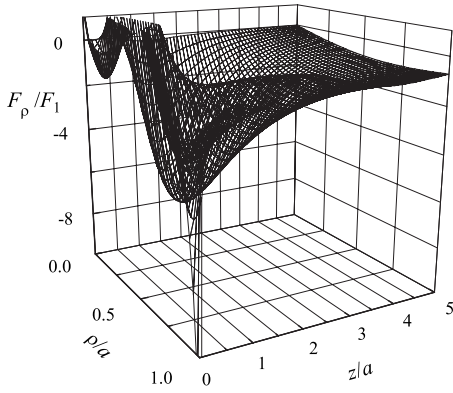


FIG. 9. Radial component of the gradient force in case of the Fresnel-atom microlens as a function of coordinates at $ka=10$.

oms which interact with far-detuned laser light at dipole transition $5^2S_{1/2}(F=3) \rightarrow 5^2P_{3/2}(F=4)$ with wavelength $\lambda = 780$ nm. For this transition, the natural linewidth is $2\gamma = 2\pi \times 5.98$ MHz and the saturation intensity is $I_S = 1.6$ mW/cm².

A. Bethe-atom microlens

Figure 10(a) shows trajectories of the atoms in the beam before and after focusing by the Bethe-atom microlens. It can be seen from the figure that the Bethe-atom microlens focuses atoms to a small spot. At the same time, it can be seen from Fig. 10(a) that periphery atoms in the beam are focused

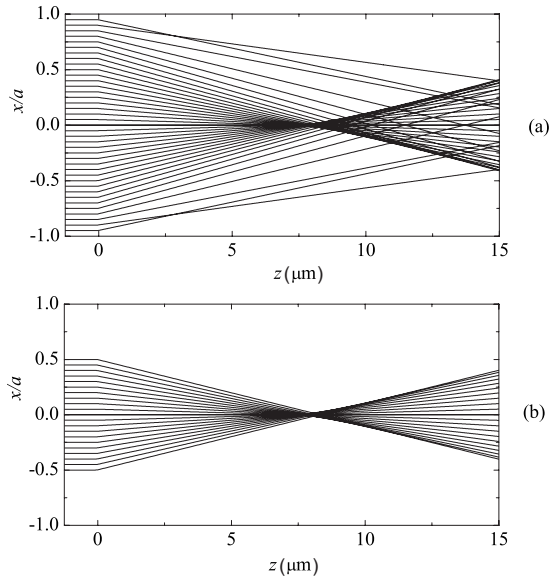


FIG. 10. (a) Atom trajectories in the atomic beam focused by the Bethe-atom microlens. The screen with a round aperture of a relative size $ka=0.25$ is illuminated by a circularly polarized light wave at detuning $\delta=-300\gamma$ and intensity $I=25$ W/cm². The longitudinal velocity of atoms is $V=5$ m/s. (b) Atom trajectories in the same Bethe-atom microlens in the case of blocking of the periphery atoms by an additional screen with a round aperture of radius $r=0.5a$.

at large distances, thus smearing the focusing region. However, this disadvantage of the atomic microlens can easily be eliminated by blocking periphery atoms of the beam with an opaque screen as shown in Fig. 10(b).

A simple estimate of the focal length of the Bethe-atom microlens can be obtained on the basis of the magnitude of the gradient force near the optical axis. Considering that the radial force acts in the region with approximate length $\delta z \approx 2a$ and has an approximate value $F_\rho \approx 2F_0$, one can estimate the variation in the transverse atomic velocity during the time of flight $\tau_{fl} \approx 2a/V$ through the microlens as

$$\delta v_\rho \approx \frac{4F_0 a}{M V}.$$

On the other hand, this variation in transverse atomic velocity leads to a deviation of the atomic trajectory by the angle defined by the ratio of the transverse coordinate to the focal length f :

$$\frac{\delta v_\rho}{V} \approx \frac{a}{f}.$$

The above relations show that the focal length of the Bethe-atom microlens can be estimated as

$$f \approx \frac{MV^2}{4F_0}, \quad (64)$$

where quantity F_0/M defines the typical value of acceleration due to the radial force.

Applying the above evaluation to the ⁸⁵Rb atomic beam propagating with longitudinal atomic velocity $V=5$ m/s through the aperture with radius $a=0.08$, $\lambda=0.06$ μ m one can see that at laser wave intensity $I=25$ W/cm² and detuning $\delta=-300\gamma$ the focal length is estimated as $f \approx 5$ μ m. Note finally that, in accordance with estimate (64), one of the main factors limiting the size of the focal spot is the velocity spread of the atomic beam. Simple geometrical considerations show that at a given relative velocity spread $\alpha = \Delta V/V$ the spot size at the focus amounts to a value of the order of $2\alpha a$. For example, for velocity spread $\alpha=10^{-2}$ the spot size at the focus constitutes a few nanometers. Diffuse broadening of the focal spot due to photon recoil fluctuations amount to an even smaller value owing to a short time of flight of atoms through the region of focusing field. For example, for the above parameters of the atomic microlens, the time of flight of an atom through the focusing field region amounts to $\tau_{fl} \approx 2a/V \approx 10^{-8}$ s. The velocity diffusion coefficient, which is defined as $D = \gamma v_r^2 (I/I_S) (\gamma/\delta)^2$, where $v_r = \hbar k/M$ is the recoil velocity, has a value of $D \approx 0.8 \times 10^6$ cm²/s³. Accordingly, the broadening of the transverse velocity distribution due to photon recoil is about $\Delta v_\rho = \sqrt{D \tau_{fl}} \approx 0.1$ cm/s and spatial broadening $\Delta \rho \approx \Delta v_\rho \tau$ of the beam in transverse direction is of the order of $\Delta \rho \approx 5 \times 10^{-3}$ nm. At last, for the chosen velocity of the atomic beam the de Broglie wavelength of the atom is as small as $\lambda_{DB} = h/p \approx 0.1$ nm. All the above estimates thus show that the focal spot size of the Bethe-atom microlens can be of the order of a few nanometers.

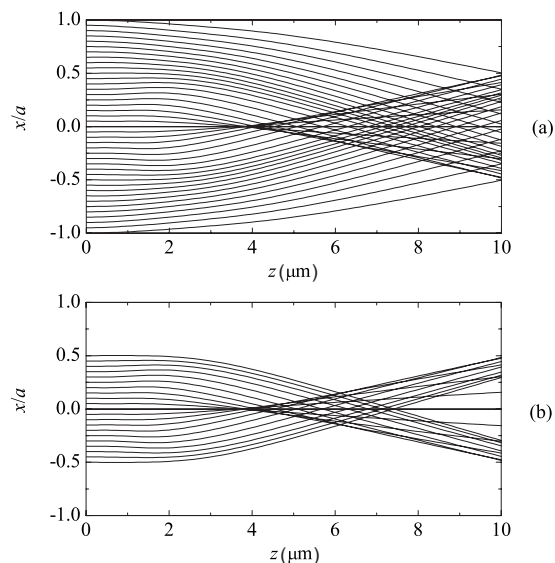


FIG. 11. (a) Atom trajectories in an atomic beam focused by the Fresnel-atom microlens with relative aperture $ka=10$ at detuning $\delta=-300\gamma$, laser light intensity $I=25$ W/cm², and longitudinal atomic beam velocity $V=5$ m/s. (b) Atom trajectories when the outer part of the atomic beam is blocked by the screen with aperture of radius $r<0.5a$ for the same parameters as in (a).

B. Fresnel-atom microlens

Figure 11(a) shows the trajectories of the atoms in the beam focused by the Fresnel-atom microlens. As one can see, under the same parameters as for the Bethe microlens the Fresnel microlens gives much larger focusing area. This is naturally explained by a relatively large anharmonic part of the gradient force for the Fresnel microlens. This drawback of the Fresnel microlens can be only partly eliminated by blocking the outer part of the beam by an additional diaphragm as shown in Fig. 11(b).

Basic analytical estimations for the Fresnel-atom microlens are as follows. According to Eq. (61) the value of the focusing force in the region of the effective action $0 < z < 3a$ is

$$F_{\rho} \approx -\kappa_0 \rho,$$

where the spring constant can be estimated at average value of the longitudinal coordinate $z \approx 3a$ as

$$\kappa_0 \approx \frac{\pi I}{3\omega_0} \frac{\gamma}{|\delta|}.$$

By making use of this value of the radial force one can evaluate the oscillation frequency as

$$\Omega \approx \sqrt{\frac{\kappa_0}{M}} = \sqrt{\frac{\pi I}{3M\omega_0}} \frac{\gamma}{|\delta|},$$

where M is the atom mass. At a given oscillation frequency the focus f of the Fresnel-atom microlens is defined by the quarter of the oscillation and depends on the longitudinal atomic velocity V ,

$$f \approx \frac{\pi V}{2\Omega} = \frac{V}{2} \sqrt{\frac{3\pi M\omega_0}{I}} \frac{|\delta|}{\gamma}. \quad (65)$$

For a beam of ⁸⁵Rb atoms at laser intensity $I=25$ W/cm², detuning $\delta=-10^3\gamma$, and at longitudinal velocity $V=5$ m/s focal length is estimated as $f \approx 8$ μ m which is very close to the value coming from numerical evaluations of Figs. 11(a) and 11(b).

The main factor which limits the spot size of the Fresnel-atom microlens is the anharmonicity of the gradient force. Accordingly, even for monochromatic atomic beam the spot size of the Fresnel-atom microlens only in a few times less than the transverse size of the initial beam.

VI. CONCLUSION

The above analysis shows that even though both the Bethe-atom microlens and the Fresnel-atom microlens can perform focusing of atomic beams, only the Bethe microlens can produce sharp enough focusing. In the case of the Fresnel-atom microlens the focusing is not effective due to a high degree of anharmonicity of the gradient force.

The focal length of the Bethe-atom microlens is mainly determined by the longitudinal velocity of the atomic beam, the laser light intensity and the detuning from the atomic transition frequency. The focal spot size of the Bethe microlens is mainly determined by the velocity spread of the atomic beam, as well as the factors depending on the beam quality, e.g., finite divergence and spatial inhomogeneity of the beam. The estimates show that under reasonable experimental conditions the focal spot size of the Bethe microlens can be on the order of a few nanometers. A more detailed analysis of the Bethe-atom microlens must naturally take into account the limitations imposed by the dipole-dipole interaction between the atoms as well as finite value of the atomic de Broglie wavelength [17,31].

ACKNOWLEDGMENTS

This work was supported in part by the Russian Fund for Basic Research under Grant Nos. 05-02-16370-a, 06-08-01299-à, 07-02-00748-a, and CRDF under Grant No. RU-P1-2572-TR-04.

- [1] J. E. Bjorkholm, R. R. Freeman, A. Ashkin, and D. B. Pearson, Phys. Rev. Lett. **41**, 1361 (1978).
 [2] J. E. Bjorkholm, R. R. Freeman, A. Ashkin, and D. B. Pearson, Opt. Lett. **5**, 111 (1980).

- [3] V. I. Balykin and V. S. Letokhov, Opt. Commun. **64**, 151 (1987).
 [4] V. I. Balykin and V. S. Letokhov, Sov. Phys. JETP **67**, 78 (1988).

- [5] G. M. Gallatin and P. L. Gould, *J. Opt. Soc. Am. B* **8**, 502 (1991).
- [6] J. J. McClelland and M. R. Scheinfein, *J. Opt. Soc. Am. B* **8**, 1974 (1991).
- [7] M. Prentiss *et al.*, *Appl. Phys. Lett.* **60**, 1027 (1992).
- [8] J. L. Cohen, B. Dubetsky, and P. R. Berman, *Phys. Rev. A* **60**, 4886 (1999).
- [9] T. Sleator, T. Pfau, V. Balykin, and J. Mlynek, *Appl. Phys. B: Lasers Opt.* **54**, 375 (1992).
- [10] G. Timp, R. E. Behringer, D. M. Tennant, J. E. Cunningham, M. Prentiss, and K. K. Berggren, *Phys. Rev. Lett.* **69**, 1636 (1992).
- [11] J. J. McClelland, R. E. Scholten, E. C. Palm, and R. J. Celotta, *Science* **262**, 877 (1993).
- [12] R. W. McGowan, D. M. Giltner, and S. A. Lee, *Opt. Lett.* **20**, 2535 (1995).
- [13] R. Gupta, J. J. McClelland, P. Marte, and R. J. Celotta, *Phys. Rev. Lett.* **76**, 4689 (1996).
- [14] R. J. Celotta, R. Gupta, R. E. Scholten, and J. J. McClelland, *J. Appl. Phys.* **79**, 6079 (1996).
- [15] U. Drodofsky *et al.*, *Microelectron. Eng.* **30**, 383 (1996).
- [16] M. Mützel, D. Haubrich, and D. Meschede, *Appl. Phys. B: Lasers Opt.* **70**, 689 (2000).
- [17] V. I. Balykin, V. G. Minogin, and V. S. Letokhov, *Rep. Prog. Phys.* **63**, 1429 (2000).
- [18] V. Balykin, V. Klimov, and V. Letokhov, *J. Phys. (France)* **4**, 1981 (1994).
- [19] V. I. Balykin, V. S. Letokhov, and V. V. Klimov, *JETP Lett.* **59**, 896 (1994).
- [20] H. A. Bethe, *Phys. Rev.* **66**, 163 (1944).
- [21] C. J. Bouwkamp, *Philips Res. Rep.* **5**, 321 (1950).
- [22] C. J. Bouwkamp, *Philips Res. Rep.* **5**, 401 (1950).
- [23] J. Meixner and W. Andrejewski, *Ann. Phys.* **442**, 157 (1950).
- [24] W. Andrejewski, *Z. Angew. Phys.* **5**, 178 (1953).
- [25] Y. Nomura and S. Katsura, *J. Phys. Soc. Jpn.* **10**, 285 (1955).
- [26] Y. Leviatan, *J. Appl. Phys.* **60**, 1577 (1986).
- [27] V. V. Klimov and V. S. Letokhov, *Opt. Commun.* **106**, 151 (1994).
- [28] H. Osterberg and L. W. Smith, *J. Opt. Soc. Am.* **51**, 1050 (1961).
- [29] A. S. Marathay and J. F. McCalmont, *J. Opt. Soc. Am. A* **21**, 510 (2004).
- [30] S. Chang and V. Minogin, *Phys. Rep.* **365**, 65 (2002).
- [31] E. Moreno, A. I. Fernandez-Dominguez, J. Ignacio Cirac, F. J. Garcia-Vidal, and L. Martin-Moreno, *Phys. Rev. Lett.* **95**, 170406 (2005).